AD-A162 130 NUMERICAL SIMULATION OF UNSTEADY THREE-DIMENSIONAL TURBULENT STRUCTURES I (U) SCIENTIFIC RESEARCH ASSOCIATES INC GLASTONBURY CT N S LUI ET AL 15 MAY 85 1/1

UNCLASSIFIED R85-910011-F AFOSR-TR-85-1059 F/G 20/4 NL

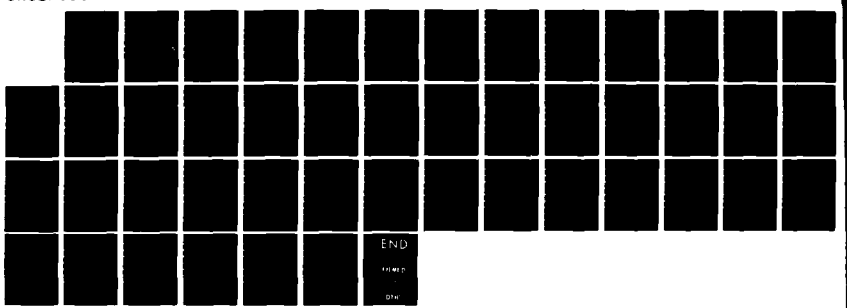

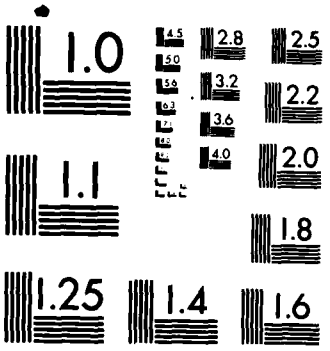

MICROCOPY RESOLUTION TEST CHART
NATIONAL BUREAU OF STANDARDS-1963-A

AFOSR SBIR PHASE I

Final Technical Report R85-910011-F

Numerical Simulation of Unsteady Three-Dimensional Turbulent Structures in Boundary Layer Flows

N.-S. Liu
S.J. Shamroth
H. McDonald

Scientific Research Associates, Inc.
Glastonbury, Connecticut

Prepared for AFOSR
under Contract F49620-84-C-0107

APPENDIX B
DOD No. 84.1

U.S. DEPARTMENT OF DEFENSE

SMALL BUSINESS INNOVATION RESEARCH PROGRAM
PHASE 1—FY 1984
PROJECT SUMMARY

Topic No. 144 Military Department/Agency Air For

Name and Address of Proposer

SCIENTIFIC RESEARCH ASSOCIATES, INC.
P.O. BOX 498
GLASTONBURY, CT 06033

Name and Title of Principal Investigator

HENRY MCDONALD, President

Proposer's Title

Numerical Simulation of Unsteady Three-Dimensional Turbulent Structures in Boundary Layer Flows

Technical Abstract (Unclassified) (Limit To Two Hundred Words)

Under a Phase I SBIR effort the capabilities for numerical simulations of the dynamical effects of the underlying structures occurring in turbulent boundary layers have been developed. A mathematically operational model of hairpin vortex, which closely resembles the experimentally observed underlying structure of wall turbulence has been constructed and the evolution of this incipient hairpin vortex as well as the distortion of a background laminar boundary layer has been successfully simulated. The height of the incipient hairpin vortex is about 1/5 of the local boundary layer thickness. The calculated results not only exhibit most of the prominent features associated with turbulent spots and turbulent boundary layer flows, but also reveal dynamical processes which have been very difficult to observe in experimental studies, notably, the formation and intensification of another counter rotating hairpin vortex immediately upstream of the incipient hairpin vortex.

Anticipated Benefits/Potential Commercial Applications of the Research or Development

The proposed effort has demonstrated the potential to use the numerical simulation as a tool to investigate the unsteady flow characteristics of turbulent boundary layer flows. It would provide new insights into the boundary layers per se, and would be very helpful in interpreting and correlating various features observed in experiments. Furthermore, it would lead to the exploiting of methods for controlling turbulence characteristics. Later phases of this work would yield useful information about the unsteady flow characteristics pertaining to the improvement of the performance of stalled airfoils.

SECURITY CLASSIFICATION OF THIS PAGE

REPORT DOCUMENTATION PAGE

1a. REPORT SECURITY CLASSIFICATION: Unclassified	1b. RESTRICTIVE MARKINGS
2a. SECURITY CLASSIFICATION AUTHORITY	3. DISTRIBUTION/AVAILABILITY OF REPORT: Approved for public release, distribution unlimited
2b. DECLASSIFICATION/DOWNGRADING SCHEDULE	
4. PERFORMING ORGANIZATION REPORT NUMBER(S): R85-910011-F	5. MONITORING ORGANIZATION REPORT NUMBER(S): AFOSR-TR- 85-1059
6a. NAME OF PERFORMING ORGANIZATION: Scientific Research Associates; 6b. OFFICE SYMBOL (If applicable):	7a. NAME OF MONITORING ORGANIZATION: Air Force Office of Scientific Research
6c. ADDRESS (City, State and ZIP Code): P.O. Box 498, Glastonbury, CT 06033	7b. ADDRESS (City, State and ZIP Code): Building 410, Bolling AFB, DC 20332-6448
8a. NAME OF FUNDING/SPONSORING ORGANIZATION: Air Force Office of Scientific Research; 8b. OFFICE SYMBOL (If applicable): AFOSR/NA	9. PROCUREMENT INSTRUMENT IDENTIFICATION NUMBER: F49620-84-C-0107
8c. ADDRESS (City, State and ZIP Code): Building 410, Bolling AFB, DC 20332-6448	10. SOURCE OF FUNDING NOS.

PROGRAM ELEMENT NO.	PROJECT NO.	TASK NO.	WORK UNIT NO.
61102F	2307	A1	

11. TITLE (Include Security Classification): Numerical Simulation of Unsteady 3D Turbulent Structures in Boundary Layer Flows (Unclassified)

12. PERSONAL AUTHOR(S): Liu, Nan-Suey; Shamroth, Stephen J.; and McDonald, Henry

13a. TYPE OF REPORT	13b. TIME COVERED	14. DATE OF REPORT (Yr., Mo., Day)	15. PAGE COUNT
Final	FROM 11/84 TO 5/85	85/5/15	42

16. SUPPLEMENTARY NOTATION: Technical Monitor Dr. James Wilson/Major Michael Francis

17. COSATI CODES		
FIELD	GROUP	SUB. GR.

18. SUBJECT TERMS (Continue on reverse if necessary and identify by block number): Numerical Simulation, Coherent Wall Structure, Navier-Stokes Equations

19. ABSTRACT (Continue on reverse if necessary and identify by block number)

Under a Phase I SBIR effort the capabilities for numerical simulations of the dynamical effects of the underlying structures occurring in turbulent boundary layers have been developed. A mathematically operational model of hairpin vortex, which closely resembles the experimentally observed underlying structure of wall turbulence, has been constructed and the evolution of this incipient hairpin vortex as well as the distortion of a background laminar boundary layer has been successfully simulated. The height of the incipient hairpin vortex is about 1/5 of the local boundary layer thickness. The calculated results not only exhibit most of the prominent features associated with turbulent spots and turbulent boundary layer flows, but also reveal dynamical processes which have been very difficult to observe in experimental studies, notably, the formation and intensification of another counter rotating hairpin vortex immediately upstream of the incipient hairpin vortex.

20. DISTRIBUTION/AVAILABILITY OF ABSTRACT	21. ABSTRACT SECURITY CLASSIFICATION
UNCLASSIFIED/UNLIMITED ☒ SAME AS RPT ☐ DTIC USERS ☐	Unclassified

22a. NAME OF RESPONSIBLE INDIVIDUAL	22b. TELEPHONE NUMBER (Include Area Code)	22c. OFFICE SYMBOL
JAMES D WILSON	(202) 767-4935	AFOSR/NA

DD FORM 1473, 83 APR EDITION OF 1 JAN 73 IS OBSOLETE

SECURITY CLASSIFICATION OF THIS PAGE

TABLE OF CONTENTS

	Page
INTRODUCTION	1
ANALYSIS	3
Hairpin Vortex as Structure of Wall Turbulence	3
The Governing Equations	5
A Model of the Hairpin Vortex	10
Initial and Boundary Conditions	15
The Solution Procedure	18
CURRENT EFFORTS	21
Objective	21
Outlines of the Simulation	21
Results	23
ESTIMATES OF TECHNICAL FEASIBILITY	30
CONCLUDING REMARKS	31
REFERENCES	32
FIGURES	35

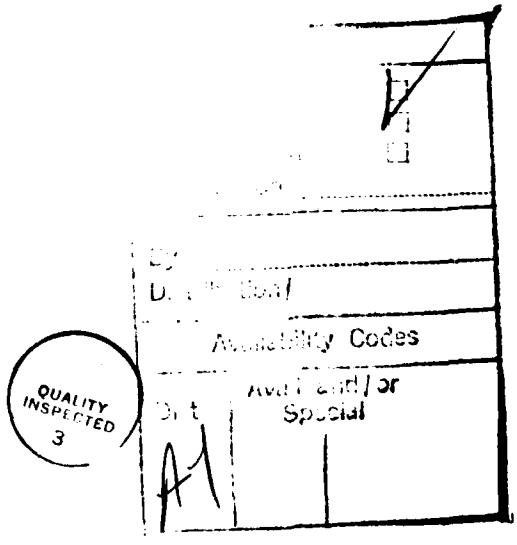

INTRODUCTION

The coherent structures in turbulent flows have been under intense investigation in recent years. These large-scale structures exhibit unsteadiness in background flows which are nominally steady, and their existence has been noted in free shear layers [1], turbulent spots [2], and wall boundary layers [3]. For wall bounded shear flows, there is strong evidence that the commonly observed large-scale features could well be the result of a colony of fine-scale hairpin vortices which, when ensemble-averaged, produce the observed mean turbulent flow. These investigations focused upon the naturally occurring turbulent structures. On the other hand, motivated by the potential applications of forced, unsteady vortex generation to the improvement of efficiency and performance of various aerodynamic devices [4], vortex structures with scales greater than the scales of the boundary layers were artificially generated near the wall and the evolution of these structures were experimentally investigated [5]. It is interesting to note that, although the scales involved are entirely different, the general geometry and deformation of the forced structures reported in Ref. [5] are quite similar to those of hairpin vortices naturally occurring in the near wall region.

Thus, an investigation of the essential features associated with the induced flow fields of hairpin vortices and the study of their dynamics in various background flows is important not only in understanding the turbulent flows per se, but also in exploiting the unsteady flow characteristics that may improve aerodynamic efficiency and enhance component performance through modification of the turbulence characteristics.

Under the premise that a mathematically operational model of hairpin vortex can be constructed, the hairpin vortex can be used in different contexts to study various aspects associated with turbulent boundary layer flows. For example, the turbulent boundary layer might be simulated by an appropriate ensemble of hairpin vortices, then the dynamics of these vortices could be tracked either in Lagrangian reference frames by methods described in [6] or in an Eulerian reference frame by using continuity and momentum equations. However, at the present stage of the development of the hairpin vortex concept, it is felt that more fruitful insights could be obtained by pursuing in the directions of two distinct but related approaches, namely, (i) the

investigation of the dynamics of one or several separated representative hairpin vortices submerged in various background boundary layer flows which can be laminar or turbulent, with or without pressure gradients, and (ii) the construction of useful statistical models using hairpin vortices to provide a quantitative link between mean flow properties and turbulence properties. The latter approach is a synthesis approach and, therefore, is inherently kinematic in its nature. When pursuing the synthesis approach, the dynamic information is indirectly included through the specifications of the structural parameters of the modelling vortices. Obviously, these two approaches are complementary with each other, the experiences gained in one approach can be used to advance the other's development.

A preliminary assessment of a synthesis approach has been made in [7], and the results indicate that the application of the proposed synthesis technique to estimate statistical properties of turbulent boundary layer flows via hairpin vortex model of wall turbulence is quite feasible. The present work focuses upon the development of capabilities for investigating the dynamic evolution as well as the effect of hairpin vortices submerged in various background flows by numerical simulation through the solution of unsteady, three-dimensional Navier-Stokes equations. As an initial effort, the case of a representative hairpin vortex submerged in a laminar boundary layer flow (Blasius flow) is numerically investigated, the initial height of the vortex is about 1/5 of the local boundary layer thickness. The calculated results not only exhibit most of the prominent features associated with turbulent spots and turbulent boundary layer flows, as identified before by other investigators, but also reveal dynamical processes which have been very difficult to observe in experimental studies, as limited by the nature of their sampling and identification techniques.

ANALYSIS

As previously discussed, numerical simulation of a hairpin vortex immersed in a wall shear flow can be used both to study the basic mechanisms of turbulent flow as well as to develop methods for exploiting unsteady flow features to influence turbulence characteristics. As was shown in Ref. 5, the structures of forced vortices generated to increase aerodynamic performance are very similar to those naturally occurring in boundary layer coherent structures. Therefore, a discussion of previous experimental and analytical studies focusing upon hairpin vortices as the basic structure of wall turbulence serves as relevant background material for the present Phase I effort which could be extended either to investigate the basic structure of turbulent wall layers or to investigate the dynamics of large scale vortices immersed in a shear flow.

Hairpin Vortex as Structure of Wall Turbulence

The concept of modelling the turbulent boundary layer with a random array of hairpin vortices was first suggested by Theodorsen [8] in 1955 and has subsequently been considered by many other workers (see, e.g. [9]). These earlier proposals tended to be rather in the nature of intuitively appealing hypotheses, supported only indirectly by experimental evidence. However, very convincing evidence for the existence of these vortices has been reported over the past five years by a large number of investigators using different techniques to study various features associated with the underlying structures of wall turbulence. A comprehensive account of these results will not be given here, nevertheless, selected works are cited to indicate the current status of the knowledge of the structure of turbulent boundary layer.

Experiments of Head and Bandyopadhyay [3] have provided very strong support for the hairpin vortice as a deterministic structure in turbulent boundary layers. Flow visualization studies of the zero pressure gradient turbulent boundary layer at Reynolds numbers up to $Re_\theta \approx 10^4$ have shown that a turbulent boundary layer consists of a forest of hairpin vortices which are undergoing a stretching motion under the influences of the self-induced field as well as the pre-existing mean shear field. These stretched hairpin vortices

are substantially straight over a large portion of their length and inclined in the downstream direction at a characteristic angle of approximately 45° to the wall. The lateral dimensions of these vortices are suggested to follow the Kline scaling, while their length appears to be limited only by the thickness of the layer. There is considerable evidence that these vortices originate from the longitudinal vortex motions in, or very close to, the viscous sublayer.

Combining anemometry and flow visualization, Falco [10] established that all of the structural features of turbulent boundary layers, e.g., the sweep and ejection events, identified before by other investigators can be associated with the evolution of a so-called pocket flow module, in which a hairpin vortex is formed and then dominates the flow behavior over a time duration extending over at least half of the flow module's life time. In Ref. [11] Dinkelacker evaluated results compiled from several measurements of wall pressure fluctuations and suggested that an important part of the observed wall pressure patterns might be manifestations of the existence of hairpin vortices in the turbulent boundary layer flow.

The above experimental studies provide strong evidence for the existence of hairpin vortices as one of the dominant structures in wall-bounded turbulent flows. However, as limited by the nature of their sampling and identification techniques, the hairpin vortex has only been indirectly observed in a turbulent boundary layer; i.e., the response of the visual indicators to the velocity field is observed. In addition, the probe data are limited by the number of spatial points at which correlations are obtained and by the small number of different quantities that can and have been measured. These deficiencies have largely been eliminated by a very recent investigation conducted by Moin and Kim [12] using a data base generated by the large-eddy simulation calculations. Two-point correlations of velocity and vorticity fluctuations strongly support a flow model consisting of vortical structures inclined at 45° to the wall. The instantaneous vorticity vectors plotted in these inclined planes show that the flow contains a large number of hairpin vortices, and vortex lines are used to display the three-dimensional structure of hairpins. In another investigation Landahl [13] modelled the dominant coherent structure near the wall with a flat eddy, which can be regarded as a first approximation to the hairpin vortex, and then examined the fundamental assumptions behind Prandtl's mixing length theory. According to Landahl the validity of two of

the main hypotheses underlying the mixing length theory has been positively confirmed with this model. Thus, this work provides an encouraging indication of the consistency of over all fluid dynamics according to the conventional mixing length model (long known to provide a remarkably accurate description of the near wall turbulent mean flow velocity) and that due to the hairpin vortex.

As mentioned before, early turbulence models based on the concept of hairpin vortex tended to be in the nature of intuitively appealing hypotheses and were mainly aimed at providing a kinematic description of the wall turbulence, as well as an explanation of some of the underlying dynamics. In the light of recent findings from experimental research on turbulent structures in the near wall region and also by using Townsend's attached-eddy hypothesis [14], Perry and his coworkers ([15], [16]) proposed a more refined hairpin vortex model for wall turbulence. The turbulent boundary layers are viewed as an ensemble of groups (or hierarchies) of hairpin vortices which originate from and are attached to the wall. These vortices are geometrically similar and have the same characteristic velocity scale being the wall shear velocity. The length scales of the hierarchies range from the smallest eddies having the Kline scaling to the largest eddies being of the order of the boundary layer thickness. The probability distribution for hierarchies is inversely proportional to the length scales of the hierarchies, and all the vortices lean 45° in the downstream direction. It is found that such a model gives the correct mean flow vorticity distribution. Further, by using the velocity signatures generated by hairpin vortex with the aid of the Biot-Savart law, turbulence spectral distributions are derived and, when compared with experimental results, the predicted turbulence spectra appear to have correct properties. Thus, in spite of the fact that there still exists uncertainties about the details of the formation, shape and subsequent evolution of the hierarchies of vortices, the works of Perry and his coworkers demonstrated that the use of hairpin vortices in obtaining a quantitative link between the mean flow, Reynolds shear stress, turbulence intensities and spectra as well as other statistical properties of wall turbulence looks promising.

The Governing Equations

Although the background flows can be considered as nominally steady and two-dimensional, the flow field associated with the evolving hairpin vortex is

unsteady and three-dimensional, i.e., they are accompanied by negative cross flows and possible streamwise reverse flows. Thus, governing equations derived from conventional boundary layer theory are not suitable for the purpose of studying the dynamics of hairpin vortex. An approximate form of the unsteady three-dimensional Navier-Stokes equations has been used to solve the three-dimensional time-dependent viscous flows over airfoil sections [17]. These equations are more general than the conventional boundary layer equations, notably in the inclusion of spanwise and streamwise diffusion terms, and the major assumption is that there is no pressure gradient in the direction normal to the wall. The solution of this set of governing equations is less demanding in computer resources than the solution of the full Navier-Stokes equations. Unfortunately, the assumption of zero normal pressure gradient which is inherent in this extended boundary layer approach makes it inapplicable to the present investigation. In this regard it should be noted that, associated with the presence of a hairpin vortex, there exists a corresponding three-dimensional pressure field. Further, in the proximity of the vortex, the pressure variations in all directions must be significant, unless the strength of the vortex is infinitesimal. In this sense, the existence of a hairpin vortex can be thought of as being sustained by a pressure field containing localized regions of significant gradients in all directions. The assumption that the normal pressure gradient is negligibly small throughout the entire flow field is thus contradictory to the presence of the hairpin vortex. In the following, the governing equations for the leading behavior of a vortex point in a background rotational flow field is derived by using the procedure described by Ting in [18]. This serves the dual purpose of demonstrating the role of pressure gradients as well as some dominant factors to be expected in the investigation of vortex dynamics.

Considering an initial vorticity distribution $\zeta(x,y,o)$ which consists of two parts:

$$\zeta(x,y,0) = f_1(x,y) + f_2(\bar{x},\bar{y}) \tag{1}$$

f_1 is the initial vorticity of the background rotational flow. It is distributed with the characteristic length scale L and its magnitude is of the order of U/L, where U is the characteristic velocity of the background flow. The portion f_2 represents a concentrated distribution near a point C(X(0),Y(0))

and it is of compact support or decays exponentially in $\tilde{r}$ where $\tilde{r}$ is the distance from C on a small length scale ϵL. Note that f_2 is a function of the stretched variables $\tilde{x}$ and $\tilde{y}$ with

$$\tilde{x} = \left[x - X(t)\right]/\epsilon\,, \qquad \tilde{y} = \left[y - Y(t)\right]/\epsilon \tag{2}$$

where (X(t), Y(t)) is the location of the vortex center and ϵ is a small parameter to be chosen. The total strength of f_2 is assumed to be of the order of UL, i.e.

$$\iint_{-\infty}^{\infty} f_2 \, dx\, dy = \Gamma = O(UL) \tag{3}$$

Therefore

$$f_2 = \epsilon^{-2}\tilde{f}_2 \quad \text{with} \quad \tilde{f}_2 = O(1) \tag{4}$$

i.e.

$$\zeta(x, y, 0) = f_1(x, y) + \epsilon^{-2}\tilde{f}_2(\tilde{x}, \tilde{y}) \tag{5}$$

It should be noted that $\tilde{f}_2$ decays rapidly with distance from the vortex center and, therefore, $\tilde{f}_2 = O(1)$ represents the maximum value of $\tilde{f}_2$.
To take into account the viscous effects inside the core, ϵ is chosen as

$$\epsilon = \frac{1}{\sqrt{Re}} = \sqrt{\frac{\nu}{\Gamma}} \ll 1 \tag{6}$$

where Re is the Reynolds number, ν the kinematic viscosity and Γ the circulation. The assumption that Γ=O(UL) is consistent with the hairpin vortex being a nonlinear, large scale structure in the wall region of the boundary layer flow. L is considered here as the boundary layer thickness and U being the wall frictional velocity.

Solutions of the unsteady Navier-Stokes equations with large Reynolds number subjected to the initial condition of Eq. (5) and appropriate boundary conditions are to be sought. The form of the initial data suggests that the solution is a composite of multiple length scales solutions:

$$\zeta(x, y, t; \epsilon) = \zeta_1(x, y, t; \epsilon) + \epsilon^{-2}\tilde{\zeta}_2(\tilde{x}, \tilde{y}, t; \epsilon) \tag{7}$$

such that at t=0

$$\zeta_1 = f_1(x,y) \quad \text{and} \quad \tilde{\zeta}_2 = \tilde{f}_2(\tilde{x},\tilde{y})$$

Accordingly, the velocity and pressure are expressed as

$$u(x,y,t;\epsilon) = u_1(x,y,t;\epsilon) + \epsilon^{-1}\tilde{u}_2(\tilde{x},\tilde{y},t;\epsilon) \tag{8}$$

$$v(x,y,t;\epsilon) = v_1(x,y,t;\epsilon) + \epsilon^{-1}\tilde{v}_2(\tilde{x},\tilde{y},t;\epsilon) \tag{9}$$

$$p(x,y,t;\epsilon) = p_1(x,y,t;\epsilon) + \tilde{p}_{12}(\tilde{x},\tilde{y},t;\epsilon) + \epsilon^{-1}\tilde{p}_{21}(\tilde{x},\tilde{y},t;\epsilon) + \epsilon^{-2}\tilde{p}_2(\tilde{x},\tilde{y},t;\epsilon) \tag{10}$$

Substituting Eqs. (8)-(10) into the continuity and Navier-Stokes equations, it can be shown that the vorticity of the background flow is redistributed by the presence of the vortical structure while the dynamics of the vortical spot is controlled by several mechanisms. The most dominant mechanism is the self-induction, followed by the relative yet coupled motion between the vortex center and the local background flow; the effects of the temporal change of the structure and viscous diffusion are the least dominant ones. More specifically, with respect to an observer moving with the vortex center, the leading behavior of the evolution of the vortical spot is governed by the following equations:

$$\frac{\partial \tilde{u}_2^{(0)}}{\partial \tilde{x}} + \frac{\partial \tilde{v}_2^{(0)}}{\partial \tilde{y}} = 0 \tag{11}$$

$$\tilde{u}_2^{(0)}\frac{\partial \tilde{u}_2^{(0)}}{\partial \tilde{x}} + \tilde{v}_2^{(0)}\frac{\partial \tilde{u}_2^{(0)}}{\partial \tilde{y}} = -\frac{\partial \tilde{p}_2^{(0)}}{\partial \tilde{x}} \tag{12}$$

$$\tilde{u}_2^{(0)}\frac{\partial \tilde{v}_2^{(0)}}{\partial \tilde{x}} + \tilde{v}_2^{(0)}\frac{\partial \tilde{v}_2^{(0)}}{\partial \tilde{y}} = -\frac{\partial \tilde{p}_2^{(0)}}{\partial \tilde{y}} \tag{13}$$

where $\tilde{u}_2(0)$, $\tilde{v}_2(0)$ and $\tilde{p}_2(0)$ are the leading term of $\tilde{u}_2$, $\tilde{v}_2$ and $\tilde{p}_2$ when expanded into a power series of ε.

In view of equations (11)-(13), it is obvious that any flow simulation technique based on the assumption of zero normal pressure gradient throughout the entire flow field will immediately force a disintegration of the vortical structure, consequently, the general behavior of this structure cannot be properly studied. Based on this asymptotic analysis as well as the previously discussed physical manifestation of the existence of a concentrated vortical structure in terms of its associated pressure field, it is concluded here that Navier-Stokes equations should be used in the investigation of the dynamics of hairpin vortices. Numerical techniques for the solution of unsteady, three-dimensional Navier-Stokes equations are currently available (see e.g. [19], [20]).

The above analysis indicates that the dominant behavior of the evolution of a vortical spot is governed by steady, Euler equations written in a coordinate system attached to the vortex center. Obviously, information about the motion of the vortex center, the interactions between the vortical spot and the surrounding background flow as well as the inner strucure of the vortical spot cannot be determined by these set of leading order equations. Such information must be obtained by investigating higher order equations derived in the asymptotic analysis. Generally speaking, the motion of the center of a two-dimensional vortical spot depends on its inner structure and the local background flow situation. For the three-dimensional case, the motion of the centerline of a vortex filament further depends on the geometrical properties of the centerline.

Another interesting consequence of the above asymptotic analysis is that the frequently employed Taylor's hypothesis of frozen eddies is a valid approximation to the leading order. Hence, if the position and the associated induced velocity field of a vortical structure is known at some instant, then the dominant part of the associated pressure field can be obtained by considering the steady, Navier-Stokes equations. This frozen-eddy approximation is used here for specifying the initial pressure field associated with a representative hairpin vortex, and it is noted that the subsequent pressure fields are obtained from solving the unsteady Navier-Stokes equations.

A Model of the Hairpin Vortex

Although the present study determines the dynamic behavior of a hairpin vortex immersed in a shear flow via a solution of the time-dependent, three-dimensional Navier-Stokes equations, it is necessary to specify an initial flow field; i.e., a flow field at $t = 0$, which includes an initial vortex structure. This field is based upon a hairpin vortex model. As shown in Ref. [12], a hairpin vortex is an agglomeration of vortex lines in a compact region that have a hairpin or horseshoe shape. Equivalently, a hairpin vortex is considered here as a slender tube-like region in which the bulk of vorticity is concentrated. Over each cross-section of this tube-like region, a mean direction, $\vec{e}_s$, as well as the strength, Γ, of the concentrated vorticity can be determined. Further, inside of this compact region, a spatial curve can be found such that its tangent is parallel to $\vec{e}_s$ at each cross-section, this spatial curve is considered as the effective centerline of the slender yet highly vortical region, the position vector of this effective centerline is denoted by $\vec{r}_c$ and a segment of this line is denoted by $d\vec{s} = ds\vec{e}_s$.

When viewed from a region sufficiently away from the effective centerline, the slender hairpin vortex is reduced to a curved line vortex of strength Γ and with position vector $\vec{r}_c$. The signature of the hairpin vortex in this outer region is then the induced velocity field given by the Biot-Savart law:

$$\vec{v}(\vec{r}) = -\frac{1}{4\pi}\int_c \frac{\Gamma(\vec{r}_c - \vec{r})}{|\vec{r}_c - \vec{r}|^3} \times d\vec{s} \tag{14}$$

where $\vec{r}$ is the position vector of a point P in the space and $\vec{r}_c$ is the position vector of a point along the line vortex C.

However, when a point P is located in the proximity of the hairpin vortex, the effects of the inner structure of the vortex on the induced field must be taken into account. Although this can be accomplished by using a so-called optimum similarity solution [18] to prescribe the diffusive core structure, the present work employs a simpler model to account for the influence of the diffusive vortex core by multiplying the induced velocity obtained in Eq. (14) with a factor

$$f(d, r_0) = \frac{d^2}{d^2 + r_0^2} \tag{15}$$

where $d = |\vec{r}-\vec{r}_c|$ and r_o is the effective core radius. Note that if the solid-body-rotation model were used for simulating the core structure, the multiplying factor would be the minimum between 1 and d^2/r_o^2.

There is considerable evidence that the hairpin vortices originate from the region very close to the wall, in addition, it has been proposed that the configuration of the hairpin vortices in the wall region consists of trailing vortex pairs running along the wall and originating from initially spanwise-oriented vorticity [15]. These trailing vortex pairs often have been referred as counter-rotating vortex pairs of elongated streamwise extent in the wall region of the flow (see, e.g. [21]). These trailing vortices form dipoles of vorticity and their farfield effect is negligible. Aside from the appearance of these trailing vortex pairs in the immediate neighborhood of the wall, the hairpin vortex as a whole must induce an internal shear layer within the pre-existing boundary layer such that the induced velocity field also satisfies the non-slip condition along the wall, very little is known about the structure of this induced, unsteady internal shear layer. The present model of hairpin vortex neglects the details of the trailing vortex pairs and the induced internal shear layer in the region very close to the wall, it is assumed that the effects of their presence are to maintain the attachment of the hairpin vortex to the wall, and to provide a rapid change of the induced velocity field in the region very close to the wall such that the no-slip condition is satisfied. These effects are accounted for by including the wall images of the hairpin vortices when their associated induced velocity fields are evaluated and, in addition, by multiplying the induced velocity fields with a factor

$$g(y) = \ell(y)/\ell_o \tag{16}$$

where y is the distance from the wall and

$$\ell(y)/\ell_o = \tanh(\kappa y/\ell_o)\mathcal{D} \tag{17}$$

with

$$\mathcal{D} = 1 - \exp(-y/\ell_1) \tag{18}$$

and κ is the von Karman constant; ℓ_o and ℓ_1 are some characteristic length scales.

Such a model of induced internal shear layer is based upon Prandtl's mixing length theory which assumes that the velocity fluctuations in the near wall region are proportional to some length scale $\ell(y)$. The present work further assumes that the distribution of $\ell(y)$ is given by Eqs. (17) and (18), which are similar in their forms to the mixing length model proposed in Ref. [22], except that ℓ_o is considered here as a vertical length scale representing the conjectured thickness of the induced internal shear layer and ℓ_1 is considered here as a vertical length scale on which the near wall damping becomes important. Typically, ℓ_o can be chosen as a small fraction of the height of the hairpin vortex and ℓ_1 is approximately equal to ℓ_o. It is stressed here that this model of induced internal shear layer is used only for constructing the initial induced flow field associated with the introduced hairpin vortex, and it is not used in the subsequent calculations.

As mentioned before, the hairpin vortex has a general shape resembling a rounded-top horseshoe. The Biot-Savart integral, i.e. Eq. (14), for a curved vortex filament formally contains singular terms. Although these singular terms can be removed by analytical cancellation [18] in addition to the prescription of models of diffusive core structure such as the one given by Eq. (15), considerable mathematical and computational complexities are involved with the evaluation of the induced velocity field of a curved vortex filament. The present work assumes that the precise shape of the hairpin vortex is not of major importance; therefore, for simplicity in setting the initial flow field for the Navier-Stokes simulation the legs of the hairpin vortex will be assumed to be straight and merge at a sharp point. As for the orientation of the initial flow field hairpin vortex, the inclination angle between the vortex and the wall is mainly determined by the balance between the self-induced strain field and the strain field provided by the background flow [3]. For a hairpin vortex extending from the wall to the outer edge of the boudary layer, the inclination angle is not uniformly 45°. In the close vicinity of the wall, the inclination of the trailing vortex pairs is much smaller than the 45° angle, while near the outer edge of the boundary layer, it is much larger than the 45° angle, nevertheless, over a substantial portion of the hairpin vortex, the legs

remain essentially straight with a characteristic inclination angle of 45°. After setting this initial flow, the hairpin vortex development is governed by the solution of the three-dimensional, time-dependent Navier-Stokes equations. In addition, it is assumed that the hairpin vortices appear mostly in the form of an array in the spanwise direction, and members of the same array of vortices have identical properties. Such an assumption implies that the hairpin vortices are produced by the evolution of an initially spanwise-oriented two-dimensional vortex line into a three-dimensional wavy structure which is periodic in the spanwise direction.

Based on the above discussions, the fundamental hairpin vortex model used in the present work consists of a spanwise array of identical vortices. The effective centerline of these vortices forms an array of interconnecting isosceles triangles which are periodic in the spanwise direction. In setting the initial flow field, the strength of these vortices does not vary along the effective centerline which inclines to the wall at an angle of 45°. In order to maintain the attachment of these vortices to the rigid wall, their wall images are also included. The effects of the inner core structure of these vortices are accounted for by introducing a diffusive factor into the evaluation of the associated induced velocity field. In addition, the existence of an induced internal shear layer in the immediate neighborhood of the wall is accounted for by employing a distributive factor into the evaluation of the induced velocity field.

A schematic of the present model is shown in Fig. 1, where h_i is the height of the i-th array of hairpin vortices, λ_i the spanwise distance between the feet of the vortices, $\phi_i = \phi = 45°$ the characteristic angle and r_{oi} the radius of the effective core. The signature or the induced velocity field of the i-th array of hairpin vortices at a point P with position vector $\vec{r}$ is then given by

$$\vec{v}_i(\vec{r}) = f_i(d_i, r_{oi}) \left[-\frac{\Gamma_i}{4\pi} \oint_{c_i} \frac{(\vec{r}_{c_i} - \vec{r})}{|\vec{r}_{c_i} - \vec{r}|^3} \times d\vec{s}_i \right] g_i(y) \qquad (19)$$

with

$$f_i(d_i, r_{oi}) = \frac{d_i^2}{d_i^2 + r_{oi}^2} \tag{20}$$

and

$$g_i(y) = \tanh(\kappa y / \ell_{oi}) \left[1 - \exp(-y / \ell_{1i}) \right] \tag{21}$$

where C_i is the effective centerline of the vortices together with their wall images, and $d_i = \left| \vec{r}_{ci} - \vec{r} \right|$. The corresponding vorticity distribution is obtained from

$$\vec{\Omega}_i = \nabla \times \vec{v}_i \tag{22}$$

Obviously, when the array contains a sufficiently large number of vortices, the induced velocity field $\vec{v}_i$ and hence $\vec{\Omega}_i$ are periodic functions with spatial period λ_i. Therefore, the induced field due to such an array of vortices is completely defined by the flow field within the spanwise domain of any one member of the vortices. Henceforth, the term 'representative' hairpin vortex will be used to indicatee some particular member of the vortex array such that the point P happens to locate within the spanwise domain of this particular vortex (see Fig. 1). It should be noted that the induced flow field within a representative hairpin vortex contains not only the contribution of this vortex but also contains the contributions of all the other vortices in the same array.

Experiences indicate that, by placing approximately 30 or more vortices on each side of the representative vortex, an excellent approximation to the spanwise periodicity required by an infinite number of spanwise vortices can be achieved. In addition, the induced streamwise velocity component $\tilde{u}_i$, the induced normal velocity component $\tilde{v}_i$ and the induced pressure $\tilde{p}_i$ are symmetric about the center plane $\tilde{z} = 0$ (see Fig. 1) while the induced spanwise velocity component $\tilde{w}_i$ is antisymmetric about $\tilde{z} = 0$, where $(\tilde{x}, \tilde{y}, \tilde{z})$ is a coordinate system attached to some nominal center of the representative vortex at $t = 0$. It also can be shown that the induced field falls off rapidly in regions relatively away from the representative vortex. The vertical extent of the domain of significant influence of the representative vortex is

approximately equal to h_i, its streamwise extent is of the order of $\ell_i = h_i \cot \phi_i$, while its spanwise extent remains to be of the order of λ_i.

Initial and Boundary Conditions

At any instant, the composite flow is considered as consisting of the background flow and the variation from the background flow. Obviously, such a variation contains not only the evolution of the initially introduced hairpin vortices, but also the subsequent distortion of the background flow due to these vortices. Let (u,v,w,p) denote the Cartesian velocity components and the pressure of the composite flow observed in a ground-fixed system (x,y,z), where x is in the streamwise direction, y is the distance normal to the wall and z is in the spanwise direction, then

$$u(x,y,z,t) = u'(x,y,z,t) + U(x,y,z) \tag{23}$$

$$v(x,y,z,t) = v'(x,y,z,t) + V(x,y,z) \tag{24}$$

$$w(x,y,z,t) = w'(x,y,z,t) + W(x,y,z) \tag{25}$$

$$p(x,y,z,t) = p'(x,y,z,t) + P(x,y,z) \tag{26}$$

where U, V, W and P are the velocity components and the pressure of the background flow which is considered as nominally steady. The variations from the background flow are denoted by (u',v',w',p').

Solutions of the governing equations with large Reynolds number and low freestream Mach number subjected to prescribed initial condition, and appropriate boundary conditions are sought by numerical solution procedure. Generally speaking, the initial conditions as well as the boundary conditions depend on the initial arrangement of the introduced hairpin vortices. The current effort focuses upon the dynamical effects of one 'representative'

hairpin vortex submerged in a two-dimensional background flow of boundary layer type. In the following, the initial condition and the boundary conditions for this case are discussed.

The background flow is supplied by performing the usual Navier-Stokes calculation for obtaining boundary layer type of flow which can be laminar or turbulent, with or without significant pressure gradient. The initial, induced velocity field associated with the introduced representative hairpin vortex is constructed with the aid of Biot-Savart law, supplemented by modifications accounting for the effects of diffusive vortical core and the effects of induced internal shear layer, as described by Eq. (16). Since the induced velocity is obtained with Biot-Savart integral, this field is evaluated with respect to a coordinate system $(\tilde{x},\tilde{y},\tilde{z})$ which is attached to some nominal center of the hairpin vortex. Note that this center can be in motion. It is assumed here that, at $t = 0$, a fixed hairpin vortex is suddenly introduced into some region of the background flow such that

$$u'(x,y,z,t=0) = \tilde{u}(\tilde{x},\tilde{y},\tilde{z}) \tag{27}$$

$$v'(x,y,z,t=0) = \tilde{v}(\tilde{x},\tilde{y},\tilde{z}) \tag{28}$$

$$w'(x,y,z,t=0) = \tilde{w}(\tilde{x},\tilde{y},\tilde{z}) \tag{29}$$

with

$$x = \tilde{x} + x_o \tag{30}$$

$$y = \tilde{y} \tag{31}$$

$$z = \tilde{z} \tag{32}$$

i.e. this initially fixed nominal vortex center is located at the midpoint between the two feet of the hairpin vortex, and it has a streamwise position $x = x_o$. As mentioned before, $\tilde{u}$, $\tilde{v}$ and $\tilde{w}$ are obtained from Eq. (19).

Thus, the incipient conditions for u, v and w are completely prescribed. The incipient condition for the composite pressure field p must be specified in

such a way that it is consistent with the prescribed composite velocity field. By noting that (i) the induced field falls off rapidly in regions away from the hairpin vortex, and (ii) over a very short time span $\Delta t \to 0$; it is quite valid to consider the induced field as frozen, then, the starting pressure field of the composite flow is obtained by using the prescribed velocity field and by integrating the normal momentum equation in its steady form subjected to the following boundary condition

$$p(x,y \to \infty,z,t = 0) = P(x,y \to \infty,z) \tag{33}$$

i.e. $p' \to o$ as $y \to \infty$

A consistent, incipient density field of the composite flow also must be supplied. In general,, this can be accomplished by several iterations between the results of the integration of the normal momentum equation and the solutions of the equation of state. For nearly incompressible flow cases, such an iteration procedure usually can be by-passed.

As for the boundary conditions, non-slip condition is applied on the wall plane and the density on this plane is calculated from the normal momentum equation. On a plane which is parallel to the rigid wall, and is located sufficiently away from the outer edge of the boundary layer, the pressure distribution is specified and the second derivative of the normal velocity component is considered as zero. In addition, the first derivatives of the streamwise as well as the spanwise velocity components are set to be zero. The streamwise boundary conditions used in the present simulation specify upstream total pressure and downstream static pressure distributions. The upstream total pressure together with specified boundary layer thicknesses and dimensionless boundary layer profiles determine the actual values of the streamwise velocity component at the inflow section. Further, the first derivatives of all the other velocity components and the static pressure are set to be zero. At the downstream boundary, the pressure distribution is specified and the second derivative of streamwise velocity component is set to be zero, while zero first derivatives of all the other velocity components are imposed on the outflow plane. These boundary conditions are expected to be appropriate so long as the inflow, outflow and the outer freestream planes are sufficiently far away from the evolving hairpin vortex throughout the course of the simulation. Due to the initial arrangement of the introduced hairpin

vortex and the use of a two-dimensional background flow, symmetrical conditions can be applied on the planes $z = -0.5\lambda$ amd $z = 0$ (see Fig. 1), this completes the specification of boundary conditions in the spanwise direction.

The Solution Procedure

The unsteady, three-dimensional, compressible Navier-Stokes equations, supplemented by an equation of state and together with the constant total temperature assumption, form the system governing the flows in the present effort. The total temperature assumption was made solely to conserve computer run time and can be easily removed through inclusion of an energy equation. The specific scalar momentum equations to be solved are the x, y and z Cartesian momentum equations. The dependent variables chosen are the physical Cartesian velocities u, v, w and the density ρ. The equations are then transformed to a computational coordinate system in which the computational coordinates (ξ, η, ζ) are related to the Cartesian coordinates (x, y, z) by

$$\xi = \xi(x,y,z,t) \tag{34}$$

$$\eta = \eta(x,y,z,t) \tag{35}$$

$$\zeta = \zeta(x,y,z,t) \tag{36}$$

$$\tau = t \tag{37}$$

Since in general the computational coordinates may be a function of time with a time-dependent Jacobian, the equations are cast into the so-called 'strong conservation form'. The present effort uses a coordinate transformation in which:

$$\xi = \xi(x) \tag{38}$$

$$\eta = \eta(y) \tag{39}$$

$$\zeta = \zeta(z) \tag{40}$$

i.e, a stretched, orthogonal grid system is used. The grid transformation used is the one originally suggested by Oh [23], which allows high resolution in user specified regions. The grid points are densely packed in regions containing the initial hairpin vortex and in regions which are expected to be occupied by the evolving and convecting hairpin vortex throughout the course of the simulation. Although future efforts would include an adaptive grid capability to follow the vortex motion such as that used in [19] and [20], use of such a grid is deemed premature in the present Phase I effort. In addition, the inflow, outflow and outer freestream boundaries are placed in the far fields of the evolving vortex.

The numerical procedure used to solve the governing equations is a consistently split linearized block implicit (LBI) scheme originally developed by Briley and McDonald [24]. The method can be briefly outlined as follows: the governing equations are replaced by an implicit time difference approximation, optionally a backward difference or Crank-Nicolson scheme. Terms involving nonlinearities at the implicit time level are linearized by Taylor expansion in time about the solution at the known time level, and spatial difference approximations are introduced. The result is a system of multi-dimensional coupled (but linear) difference equations for the dependent variables at the unknown or implicit time level. To solve these difference equations, the Douglas-Gunn procedure for generating alternating-direction implicit (ADI) schemes as perturbations of fundamental implicit difference schemes is introduced in its natural extension to systems of partial differential equations. This technique leads to systems of coupled linear difference equations having narrow block-banded matrix structures which can be solved efficiently by standard block-elimination methods.

One major problem in calculating high Reynolds number flows using the Navier-Stokes equations is the appearance of spatial oscillations associated with the so-called central difference problem. When spatial derivatives are represented by central differences, high Reynolds number flows can exhibit a saw tooth type oscillation in regions of intense flow gradients unless some mechanism is added to the equations to suppress their apperance.
This dissipation mechanism can be added implicitly to the equations via the spatial difference molecule (e.g. one-sided differencing) or explicitly through addition of a specific term. The present authors favor this latter approach for two reasons. First, if a specific artificial dissipation term is added

to the equations, it is clear precisely what approximation is being made. Secondly, if a specific term is added to suppress oscillations, the amount of artificial dissipation added to the equations can be easily controlled in magnitude and direction so as to add the minimum amount necessary to suppress spatial oscillations. Studies can also be easily performed to evaluate the effect of the explicitly added dissipation on the solution. Obviously, the most desirable technique would add only enough dissipative mechanism to suppress oscillations without deteriorating solution accuracy. In Refs. [19] and[20] it has been demonstrated that a second-order anisotropic artificial dissipation formulation suppressed spatial oscillations without impacting adversely on accuracy and could be used to capture the nearly normal shocks successfully. The same technique is used in the present work. In particular, no artificial dissipation is added when the local cell Reynolds number is below 20.

Another aspect of the present problem is the tracking and identification of evolving and convecting vortex structures in a general flow field. This is accomplished by first subtracting the background flow field from the calculated instantaneous composite flow data, the flow variations thus obtained then are analyzed with the orthogonal decomposition techniques proposed by Bethke and Viets [25].

CURRENT EFFORTS

Objective

The goal of the present work is to develop the capabilities for numerical simulation of the dynamical effects of the underlying structures occurring in turbulent boundary layers so that not only the turbulent flows per se can be better understood, but also that the unsteady flow characteristics, which may improve aerodynamic efficiency and enhance component performance through modification of the turbulence characteristics, can be exploited. Under the current effort in particular, the objectives are (1) to make an assessment of the important factors involved in the investigation of vortex dynamics so that the appropriate set of governing equations are chosen for the simulation, (2) to develop a mathematically operational model of hairpin vortex, which closely resembles the experimentally observed underlying structure of wall turbulence, and (3) to carry out a calculation to demonstrate the feasibility of the proposed numerical simulation. As shall be demonstrated, these objectives have been met.

Outlines of the Simulation

The unsteady, three-dimensional, compressible Navier-Stokes equations, supplemented by an equation of state and together with the constant total temperature assumption, form the system governing the flows in the pesent effort. The construction of the initially introduced hairpin vortex as well as the appropriate starting and boundary conditions for the current simulation have been discussed in detail in the previous sections, and will not be repeated here. Prior to the simulation involving the hairpin vortex, several typical laminar as well as turbulent boundary layer flows have been calculated by using the Navier-Stokes code; good numerical results have been obtained; when compared with experimental measurements.

As an initial effort, the present calculation simulates the dynamical evolution of a 'representative' hairpin vortex after it is introduced into a laminar boundary layer. Also simulated are the associated dynamical distortion of the background flow. As limited by the scope of the current effort, the simulation is carried out for the early stages of the evolution of the hairpin vortex and the distortion of the background flow.

The background flow is a zero-pressure-gradient laminar boundary layer flow with a freestream Mach number of 0.4, i.e., it is essentially a Blasius flow. For the present calculation, the reference length is 0.128m, the reference velocity is 139 m/sec, and the reference time is 0.9209×10^{-3} sec, henceforth, the discussion will be in terms of dimensionless units.

The inflow section of the computational domain is located at a place where $Re_x = 1.0364 \times 10^5$ and the outflow section is placed at $Re_x = 1.7673 \times 10^6$, where Re_x is the Reynolds number based on freestream velocity and the distance to the leading edge. Thus, the streamwise extent of the computational domain has a length of 40 δ_o, where δ_o is the boundary layer thickness at the inflow plane. In addition, the height of the computational domain is $6\delta_o$.

Then, a slanted 'representative' hairpin vortex is introduced into the inner wall region. The inclination angle is 45° toward the downstream direction, the feet of the vortex are attached to the wall at a place where $Re_x = 1.3510 \times 10^5$, the corresponding Reynolds number based on the local displacement thickness is about 635 and the local frictional velocity $U_\tau = 0.03$. The height of the incipient hairpin vortex is $h^+ = 12.5$, the spanwise spacing between the vortex feet is $\lambda^+ = 2h^+$, its streamwise extent is $\ell^+ = h^+ \cot 45° = 12.5$, and the strength of the vortex is $\Gamma^+ = 25$, where the superscript '+' indicates that the quantities are evaluated in wall units. It is noted here that the height of the vortex is about 1/5 of the local boundary layer thickness and the distance between the tip of the vortex and the outer freestream bounary is about 25 h^+. Further, the spanwise vorticity of the background flow in the region containing the incipient hairpin vortex is about 24 and is rotating in the clockwise direction. The maximum spanwise vorticity of the incipient hairpin vortex, depending on the spanwise location, ranges from 16 to 73 and is rotating in the same direction as the background vorticity. Thus, highly vortical yet compact regions are introduced into the background flow. Due to the symmetric properties of the incipient flow condition, only the solutions on one side of the center plane need to be calculated, therefore, the spanwise extent of the computational domain has a length of $0.5\lambda^+$.

The streamwise extent of the computational domain is covered by 49 grid points with 31 uniformly spaced grid points packed in a region of length $3h^+$, the distance between the inflow section and the upstream end of the highly

resolved region is about $97h^+$, and is covered by 9 grid points which are highly stretched. The distance between the outflow section and the downstream end of the highly resolved region is about $100h^+$, and is covered by 9 grid points which, again, are highy stretched. The vertical extent of the computational domain is covered by 41 grid points. Similar to the arrangement for the streamwise grid distribution, high resolution is provided for the region $y^+ \leq 4h^+$. As for the grid distribution in the spanwise direction, 13 grid points are used with clustering at both ends while uniform spacing applied in between. It is noted here that, in those high resolution regions, the grid spacing is $d^+ = 1.25$, and throughout the duration of the present simulation, the stretched and convected hairpin vortex remains in these highly resolved regions. The early stages of the dynamical variations of the composite flow are simulated over a time span of $t^+ = 4.5$. A total number of 40 time steps are carried out, the first 20 steps have a constant time increment of $\Delta t^+ = 0.375 \times 10^{-1}$, and the last 20 steps have a constant time increment of $\Delta t^+ = 0.1875$. Thus, the time accuracy and the spatial resolution of the present simulation are expected to be quite satisfactory.

Results

The present numerical simulation has generated a database containing information of the flow variations, i.e., the evolution of incipient 'representative' hairpin vortex and the change of the background boundary layer flow caused by the introduction of this vortex. This database needs to be examined in detail and the flow characteristics should be carefully analyzed. It is not only of great interest to investigate the dynamics of the hairpin vortex, but also of practical usefulness to study the changed flow characteristics of the background boundary layer flow, such as the wall pressure coefficient and friction coefficient, which are closely related to the performance of aerodynamic components. Such a detailed analysis should be carried out in the near future. Nevertheless, the following preliminary analysis indicates that these results exhibit most of the prominent features associated with the dominant structures occurring in turbulent spots and turbulent wall flows, they also reveal dynamic processes which have been very difficult to observe in experimental investigations using visualization and/or probe methods.

The results are presented in three types of planes, namely, the side view, the top view and the front view. The orientations of these planes are indicated in Fig. 1 as well as the first plot of each figure. The regions selected for presentation are those in the neighborhood of the incipient vortex. The flow variations in the outer region of the boundary layer and the upstream as well as downstream regions sufficiently far away from the incipient vortex will not be shown here. It is noted here that the streamwise location of the foot of the incipient hairpin vortex is denoted by x_o^+, this vortex has an initial height $h_o^+ = 12.5$ and an initial streamwise extent $\ell_o^+ = 12.5$. The initial spanwise distance between one foot of the vortex and its center plane ($z^+=0$) is $\lambda_o^+ = 12.5$. The vorticity of the background boundary layer flow in the region containing the incipient hairpin vortex is $\Omega_b = -24$, where the negative sign indicates that the orientation of the vorticity is in the clockwise direction. In addition, the results are presented in terms of the flow variations as defined by Eqs. (23)-(26). There are two sets of contours of vorticity variations. The first set consists of three levels of clockwise vorticity, namely 0.9, 0.6 and 0.3 of $\Omega'_{min} < 0$. The second set consists of three levels of counterclockwise vorticity, i.e., 0.3, 0.6 and 0.9 of $\Omega'_{max} > 0$. Both Ω'_{min} and Ω'_{max} are the instantaneous extremes in the depicted region. The strength of the velocity variation in that region is indicated by q'_{max} which is the maximum of the magnitudes of projected velocity vectors. For the case of the variation of the pressure coefficient, two sets of contours are used, the first one consists of 6 levels of low pressure, i.e., 0.9, 0.8, 0.7, 0.6, 0.5 and 0.4 of $Cp'_{min} < 0$, the second one consists of 6 levels of high pressure, i.e., 0.4, 0.5, 0.6, 0.7, 0.8 and 0.9 of $Cp'_{max} > 0$.

The temporal development of the flow variations occurring in two side-view planes are shown in Figs. 2 and 3. The lower boundary of the plane is located at $y^+/h_o^+ = 0.05$, the upper boundary is at $y^+/h_o^+ = 1.95$. The left boundary is at $(x^+ - x_o^+)/\ell_o^+ = -0.198$ and right boundary is at $(x^+ - x_o^+)/\ell_o^+ = 1.75$. Note that the background flow is from left to right. Fig. 2 illustrates the variations in a plane with spanwise location $2z^+/\lambda_o^+ = -0.7$, which is near one foot of the incipient hairpin vortex. The temporal as well as the spatial developments of the vorticity contours indicate that vorticity concentration region associated with the incipient hairpin vortex ($\Omega'_{min} < 0$) are undergoing the process of diffusion, stretching while moving toward

downstream. The maximum value of the clockwise vorticity is decreasing in the course of the time. Initially, there is a region of counterclockwise vorticity, which is underneath the incipient vortex and is weak relative to the main, concentrated vorticity. The maximum value of this counterclockwise vorticity remains more or less the same during the course of the time, and at $t^+ = 4.50$, it is about the same as the magnitude of the clockwise vorticity. However, the region of counterclockwise vorticity is now on top of the region of clockwise vorticity, and it is also inclined toward the downstream direction. The evolution of the flow variation is further illustrated with the projected velocity vector field. At $t^+ = 0$, it gives the appearance of a single and fairly coherent clockwise-rotating vortex, the center of this apparent vortex then travels toward downstream without lifting up from the wall. At $t^+ = 4.5$, it appears that this vortex loses its clear identity, but a much smaller and weaker counterclockwise-rotating vortex is now visible at the left bottom corner. Fig. 3 illustrates the variations in the center plane. Again, the diffusion, stretching and convection of the clockwise vorticity concentration region are obvious, and the maximum value of the clockwise vorticity is decreasing. At $t^+ = 4.50$, it appears that the clockwise vorticity region is either in the process of merging or in the process of breaking away, this can only be determined by carrying out a detailed analysis of the database. As for the region of concentrated counterclockwise vorticity, it is initially very close to the wall and has the shape of the cat's eye. In the course of the time, this vortical region is being lifted up from the wall while new regions of concentrated clockwise vorticity start to appear immediately upstream of the initially introduced hairpin vortex. This newly formed counterclockwise vortical region then intensifies and, at $t^+ = 4.5$, it becomes stronger than the initially introduced clockwise vortical region. In fact, when combined with results obtained in other side-view planes, it is quite obvious that a new hairpin vortex of opposite sign has been formed in the immediate upstream of the initially imposed hairpin vortex. The formation of such a counter-rotating hairpin vortex immediately upstream of the old hairpin vortex has been noted by Falco [10] through some weak visual evidence. The projected vector field of the velocity variation indicates the convection and lifting up of a clockwise-rotating vortex, at $t^+ = 4.5$, it becomes much less coherent, nevertheless, it is still identifiable. The existence of a counter-rotating

vortex immediately upstream of the old vortex is barely visible in this projected vector field, although it is quite clear in the vorticity field. The subsequent developments of these two counter-rotating hairpin vortices warrant future investigations, it is expected that their mutual evolutions are closely related to the breakdown of large scale structures, as they might merge with each other (pairing) through interactions and/or viscous diffusion.

The temporal evolution of the flow variations in several top-view planes are shown in Figs. 4, 5 and 6. The lower boundary of the plane is at $2z^+/\lambda_o^+ = -0.017$, which is very close to the centerline. The upper boundary is at $2z^+/\lambda_o^+ = -0.98$, which is quite near to one foot of the incipient hairpin vortex. The left boundary is $(x^+ - x_o^+)/\ell_o^+ = -0.198$ and the right boundary is at $(x^+ - x_o^+)/\ell_o^+ = 1.75$. The background flow is from left to right. Fig. 4 presents the variation of wall pressure coefficient at 5 time stations. Generally speaking, the patterns have a shape of an arrow head with a low pressure region followed by a high pressure region, and the patterns are convecting toward downstream. At $t^+ = 4.50$, the pressure variation in the plane at $y^+ = 6.25$ is also presented, when compared with the pressure variation at $y^+ = 0$, it can be shown that the gradient in the direction normal to the wall is of O(1) and, therefore, it cannot be neglected. An ensembly averaged wall pressure field associated with turbulent spots in a laminar boundary layer flow has been reported in Ref. [26], in which the ensembly averaged wall pressure patterns are given in some 'similarity' coordinates. Although it is interesting to note that the patterns described in [26] are quite similar to those depicted in Fig. 4, further comparison is needed to establish the connection between the present results and the one described in [26]. In Refs. [27] and [28], the wall pressure fluctuations associated with turbulent boundary layer flows have been experimentally investigated and attempts have been made to relate the observed pressure pattern to both wall events and the large-scale structure of the boundary layer, the results obtained in the present work should be compared in detail with the results reported in [27] and [28], so that the relationship between the wall events and the near wall pressure pattern can be better understood. Nevertheless, it is interesting to note that, in Ref. [28], a characteristic wall-pressure fluctuation pattern which is associated with the burst-sweep cycle of events in the wall region has been experimentally identified. This pattern has the form of an overpressure with a region of underpressure to

either side of it. Such an experimentally observed pressure pattern seems to be quite similar to the one indicated with $t^+ = 4.50$ and $y^+ = 6.25$ in Fig. 4.

The flow variations in 4 top view planes are presented for two time stations (Fig. 5 and 6). The vertical locations of these planes are indicated by y^+/h_o^+ which ranges from very close to the wall to about 1.3, note that h_o^+ is the height of the incipient hairpin vortex. Fig. 5 shows that, in the course of the time, the incipient vortex is diffused, the formation and intensification of new counter-rotating vorticity concentration region are also obvious, as already pointed out in Figs. 2 and 3. The evolution of the projected velocity vector field is illustrated in Fig. 6. At $y^+/h_o^+ = 0.1$, i.e., in a region very close to the wall, it appears that the foot of the incipient hairpin vortex (a clockwise-rotating vortex) is moving toward downstream while shifting toward the center plane. At $y^+/h_o^+ = 0.5$, the vortex is mainly translating in the streamwise direction, no apparent lateral motion is observed. At $y^+/h_o^+ = 0.9$, i.e., close to the tip of the incipient hairpin vortex, the vector field indicates that the incipient tip vortex is moving toward downstream while shifting outwardly. Thus, the incipient hairpin vortex which has an initial shape of a triangle is deforming while it is convecting in the downstream direction. The feet of the hairpin vortex are moving laterally toward each other, while the tip region is flattening out, i.e., the incipient hairpin vortex is changing its shape from a triangle (as imposed at $t^+ = 0$) to a Ω-shaped structure. The plot at $t^+ = 4.50$ and $y^+/h_o^+ = 0.9$ also indicates clearly that there is a counterclockwise-rotating vortex immediately upstream of the old clockwise-rotating vortex. The flow characteristics at $y^+/h_o^+ = 1.3$ change dramatically from $t^+ = 0.375$ to $t^+ = 4.50$. It appears that, at $t^+ = 4.50$, a relatively strong lateral flow is emanating from the center plane.

The features of the flow variation at 6 front-view planes are presented for two time stations in Fig. 7a, and Fig. 7b. The left boundary of the plane is at $2z^+/\lambda_o^+ = -0.017$, the right boundary is at $2z^+/\lambda_o^+ = -0.98$. The lower boundary is at $y^+/h_o^+ = 0.05$ and the upper boundary is at $y^+/h_o^+ = 1.95$. The background flow is from behind these front-view planes. The streamwise location of the plane is indicated by $(x^+ - x_o^+)/\ell_o^+$ which ranges from -0.29 to 1.80, i.e., from upstream region of the incipient hairpin vortex to the

downstream region of the incipient hairpin vortex which is inclined toward the downstream direction. The contours of vorticity variation at $t^+ = 4.5$ indicate again the existence of two counter-rotating hairpin vortices which are fairly close to each other. Furthermore, streamwise vortices have been developed in the downstream region of the incipient vortex. The plot at $(x^+ - x_o^+)/\ell_o^+ = 1.40$ indicates the lifting up of a vorticity concentration region from the wall while at $(x^+ - x_o^+)/\ell_o^+ = 1.80$, the vortical material still attaches to the wall. The projected velocity vector fields at $t^+ = 0$ and $t^+ = 4.50$ clearly indicate the ejection and sweep features occurring in these front-view planes. These features are closely associated with the bursting phenomena which is a prominent wall event [29]. By comparing the vector plots at $t^+ = 0$ and $t^+ = 4.5$ in a staggered manner, as indicated by the dotted arrow lines in Fig. 7a and Fig. 7b, it appears that the incipient hairpin vortex has been convected toward downstream direction. However, it should be noted that the choice of the staggered planes is solely for the purpose of illustration, the definite relationship between these planes is yet to be studied. Further, if the convection velocity of the incipient hairpin vortex can be considered as more or less constant, then, the streamwise vortex formed at $(x^+ - x_o^+)/\ell_o^+ = 1.8$ is most likely due to the effects induced by the incipient hairpin vortex, rather than as a direct result of the incipient vortex being convected to this location.

These results show that the current numerical simulation produces almost all of the prominent features associated with deterministic structures observed in turbulent spots and turbulent boundary layer flows. In addition, it also reveals dynamical processes which are difficult to observe in experiments, notably, the formation and intensification of a new counter-rotating hairpin vortex immediately upstream of the originally introduced vortex. It is conjectured here that these two counter-rotating hairpin vortices are closely related to the breakdown of large scale structures through their mutual interactions and viscous diffusion. There is no doubt that the diffusion, stretching and convection of the incipient hairpin vortex are primarily responsible for the observed flow variations. Nevertheless, there also exists evidence that the effects of the incipient hairpin vortex are propagating

toward regions sufficiently far away from the incipient hairpin vortex by a domino-like mechanism and these effects can be intensified in the course of the time.

The present results also clearly demonstrate that the numerical simulation through the solution of unsteady, three-dimensional Navier-Stokes equations can put together various experimentally observed features occurring in wall turbulent flows. Indeed, it appears that they can fit into a single picture which includes only one incipient hairpin vortex and does not include either the long streaky structure, or motions which scale on the overall boundary layer thickness. In particular, the experimentally observed patterns of various quantities such as velocity fluctuations and pressure fluctuations can be better related to each other by using the results generated from the present numerical simulation. Thus, the simulation capabilities developed under the current effort will also be of great use in interpreting and correlating the experimental results.

ESTIMATES OF TECHNICAL FEASIBILITY

Under the present effort, the capabilities for numerical simulation of the dynamical effects of the underlying structures occurring in turbulent boundary layers have been developed, and a calculation has been successfully carried out to demonstrate the feasibility of the proposed numerical simulation. These results are obtained by solving unsteady, three-dimensional Navier-Stokes equations which is embodied in a Navier-Stokes code developed at SRA. This code is partially vectorized and required 0.135×10^{-2} sec of CRAY CPU time per grid per time step. It is estimated that further vectorization of the code can reduce the run time by a factor of 4, thus allowing the numerical simulation to be a practical tool of studying the unsteady, three-dimensional characteristics of wall turbulence.

The numerical simulation capabilities developed under the current Phase I effort can be used in several different ways. It can be used to study the unsteady characteristics of the turbulent wall flows per se, and, when collaborating with experiments, it can be used to interprete and correlate various features obtained from the measurements. Furthermore, the numerical simulation developed under the current effort can be used to exploit the unsteady flow characteristics that may improve aerodynamic efficiency and enhance component performance through modification of turbulence characteristics. For example, the common vortex generators as experimentally identified in Ref. [5] produce vortical structures which closely resemble the hairpin vortices investigated here. These structures which energize the boundary layer and thereby avoid separation have found their applications to controlling flows on aircraft wings, enhancing reattachment on rearward facing ramps, improving mixing in dump combustors, and controlling the flow in diffusers (see Ref. [4]).

CONCLUDING REMARKS

The unsteady, three-dimensional, compressible Navier-Stokes equations together with the constant total temperature assumption have been applied to numerically simulate the dynamical evolution of an incipient 'representative' hairpin vortex immersed in a background laminar boundary layer flow as well as the associated changes of the characteristics of the background boundary layer flow due to their interaction. The present simulation has been carried out over a region of somewhat limited streamwise extent for a significant time duration, which is approximately 1/4 of the conjectured life span of the hairpin vortex. A preliminary analysis of these results shows the numerical simulation to reproduce many experimentally observed, prominent features occurring in wall turbulence. The present approach rests on the existence of incipient hairpin vortices and, therefore, is less demanding in computer resources than the large-eddy calculations. In addition, the present approach renders the identification and tracking of the fundamental, dynamical processes associated with hairpin vortices less difficult than would be a tracking in a large-eddy simulation. The results thus obtained would enhance the current understanding of the basic mechanisms of the wall turbulence and, when collaborating with experiments, would be of great help in interpreting and correlating the observed phenomena. Furthermore, the present approach would lead to the exploiting of methods for controlling turbulence characteristics pertaining to the improved performance of various aerodynamic devices. Another potential use of the presently proposed hairpin vortex model of wall turbulence is the development of a synthesis approach which uses the hairpin vortices to provide a quantitative link between mean flow properties and various near wall turbulence quantities including the Reynolds stresses and spectral information.

REFERENCES

1. Roshko, A.: Structure of Turbulent Shear Flows: A New Look. AIAA Journal, Vol. 14, No. 10, pp. 1339-1357, 1976.

2. Perry, A.E., Lim, T.T. and Teh, E.W.: A Visual Study of Turbulent Spots. J. Fluid Mech., Vol. 104, pp. 285-403, 1981.

3. Head, M.R. and Bandyopadhyay, P.: New Aspects of Turbulent Boundary-Layer Structure. J. Fluid Mech., Vol. 107, pp. 297-337, 1981.

4. Viets, H. and Palmer, G.M.: Potential Applications of Forced Unsteady Flows, U.S.A.F. Unsteady Flow Workshop, U.S.A.F. Academy, August 1983.

5. Viets, H., Bethke, R.J. and Bougine, D.: Three-Dimensional Vortex Dynamics Near a Wall. Fourth International Symposium on Turbulent Shear Flow, Karlsruhe, West Germany, September 1983.

6. Leonard, A.: Vortex Methods for Flow Simulation, J. of Comp. Physics, Vol. 37, pp. 289-335, 1980.

7. Liu, N.-S. and Shamroth, S.J.: On the Application of a Hairpin Vortex Model of Wall Turbulence to Trailing Edge Noise Prediction. SRA Report R85-900026-F. Prepared for Langley Research Center under Contract NAS1-17249.

8. Theodorsen, T.: The Structure of Turbulence, 50 Jahre Grenzchichtforschung, Ed. H. Gortler & W. Tollmien, p. 55, Braunschweig: Veiweg und Sohn, 1955.

9. Black, T.J.: Some Practical Applications of a New Theory for Wall Turbulence, Proc. 1966 Heat Transfer and Fluid Mech. Inst., Stanford University Press, 1966.

10. Falco, R.E.: A Synthesis and Model of Turbulence Structure in the Wall Region, Structure of Turbulence in Heat and Mass Transfer, Ed. Z.P. Zaric, pp. 43-57, 1982, Hemisphere Publishing Corp.

11. Dinkelacker, A.: Do Tornado-Like Vortices Play a Role in Turbulent Mixing Processes? Structure of Turbulence in Heat and Mass Transfer, Ed. Z.P. Zaric, pp. 59-72, 1982, Hemisphere Publishing Corp.

12. Moin, P. and Kim, J.: Structure of the Vorticity Field in Turbulent Channel Flow, Part I: Analysis of Instantaneous Fields and Statistical Correlations, NASA TM-86019, 1984.

13. Landahl, M.T.: Coherent Structures in Turbulence and Prandtl's Mixing Length Theory, Z. Flugwiss, Weltraumforsch, Vol. 8, pp. 233-242, 1984.

14. Townsend, A.A.: The Structure of Turbulent Shear Flow, 2nd Ed. Cambridge University Press, 1976.

15. Perry, A.E. and Chong, M.S.: On the Mechanism of Wall Turbulence, J. Fluid Mech., Vol. 119, pp. 173-217, 1982.

16. Perry, A.E., Henbest, S.M. and Chong, M.S.: Further Spectral Analysis of Smoothed-Wall Pipe Flow, Fourth International Symposium on Turbulent Shear Flow, Karlsruhe, West Germany, 1983.

17. Weinberg, B.C., McDonald, H. and Shamroth, S.J.: A Solution Procedure for Two- and Three-Dimensional Unsteady Flows, AIAA Paper 85-0298, 1985.

18. Ting, L.: Studies on the Motion and Decay of a Vortex Filament, Advances in Fluid Mechanics, Ed. E. Krause, pp. 67-105, 1980, Springer-Verlag.

19. Liu, N.-S., Shamroth, S.J. and McDonald, H.: Numerical Solution of the Navier-Stokes Equations for Compressible Turbulent Two/Three-Dimensional Flows in the Terminal Shock Region of an Inlet/Diffuser, AIAA Paper 83-1892, July 1983.

20. Liu, N.-S., Shamroth, S.J. and McDonald, H.: Dynamic Response of Shock Waves in Transonic Diffuser and Supersonic Inlet: An Analysis with the Navier-Stokes Equations and Adaptive Grid, AIAA Paper 84-1609, June 1984.

21. Blackwelder, R.F.: The Bursting Process in Turbulent Boundary Layer, Proc. Workshop on Coherent Structure of Turbulent Boundary Layers, Lehigh University, p. 211, 1978.

22. McDonald, H. and Camarata, F.J.: An Extended Mixing Length Approach for Computing the Turbulent Boundary Layer Development, Proceedings Computation of Turbulent Boundary Layers - 1968 AFOSR-IFP Standard Conference, Vol. 1, pp. 83-98, 1969.

23. Oh, Y.H.: An Analytic Transformation Technique for Generating Uniformly Spaced Computational Mesh, Final Report, NASA-Langley Research Grant NSG 1087, October, 1978.

24. Briley, W.R. and McDonald, H.: On the Structure and Use of Linearized Block Implicit Shcemes. Journal of Computational Physics, Vol. 34, pp. 54-72, 1980.

25. Bethke, R.J. and Viets, H.: Orthogonal Decomposition Techniques to Identify Convected Flow Structures. AIAA Paper No. 83-0048, AIAA 21st Aerospace Sciences Meeting, Reno, Nevada, Jan. 1983.

26. Mautner, T.S. and VAN ATTA, C.W.: An Experimental Study of the Wall-Pressure Field Assoiated With a Turbulent Spot in a Laminar Boundary Layer. J. Fluid Mech., Vol. 118, pp. 59-77, 1982.

27. Schewe, G.: On the Structure and Resolution of Wall-Pressure Fluctuations Associated With Turbulent Boundary-Layer Flow. J. Fluid Mech., Vol. 134, pp. 311-328, 1983.

28. Thomas, A.S.W. and Bull, M.K.: On the Role of Wall Pressure Fluctuations in Deterministic Motions in the Turbulent Boundary Layer. J. Fluid Mech., Vol. 128, pp. 283-322, 1983.

29. Blackwelder, R.F. and Haritonidis, J.H.: Scaling of the Bursting Frequency in Turbulent Boundary Layers. J. Fluid Mech. Vol. 132, pp. 87-103, 1983.

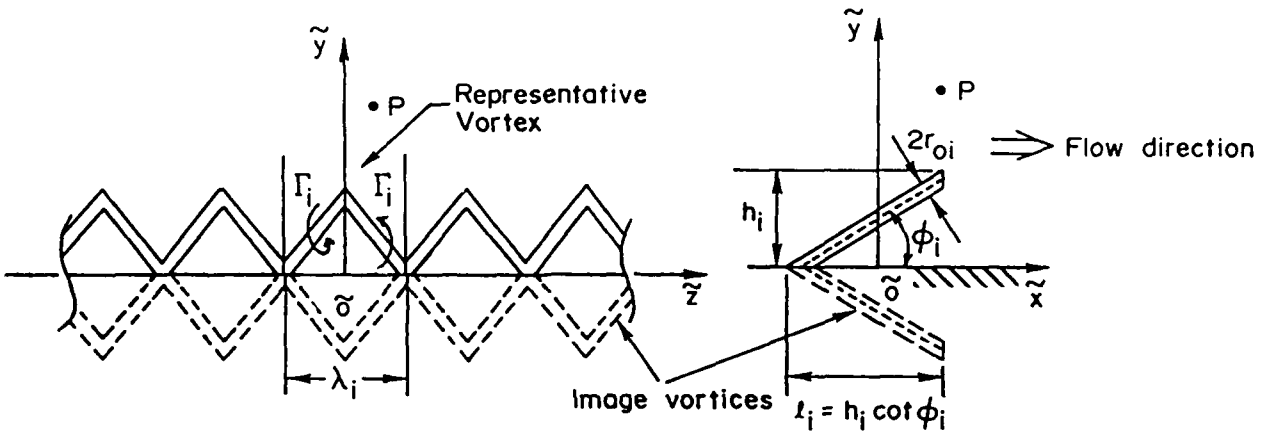

Figure 1. A schematic of an array of hairpin vortices and the representative vortex.

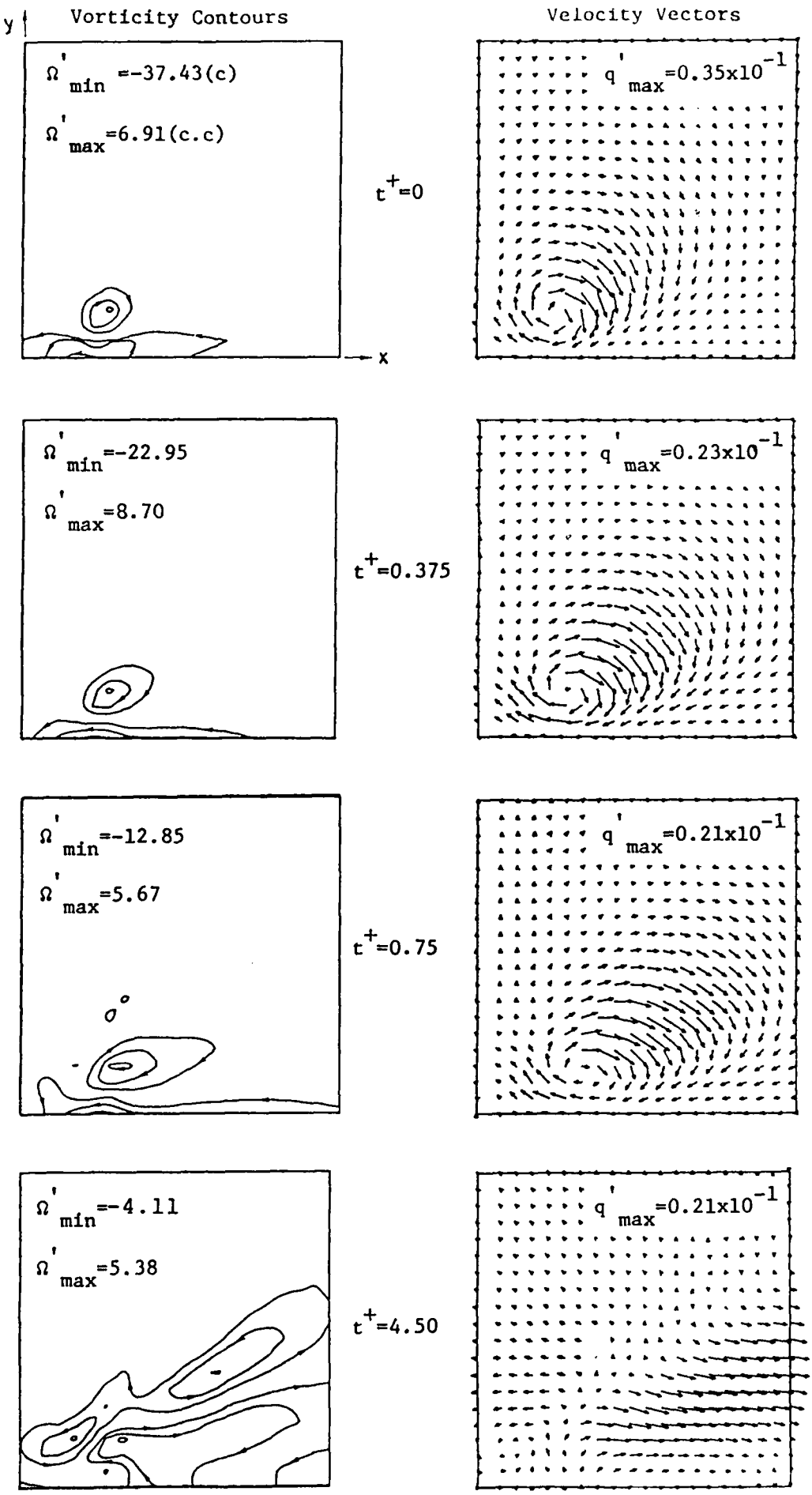

Fig.2 Variation of Flow Field (side view, $2z^+/\lambda_o{}^+=-0.7$)

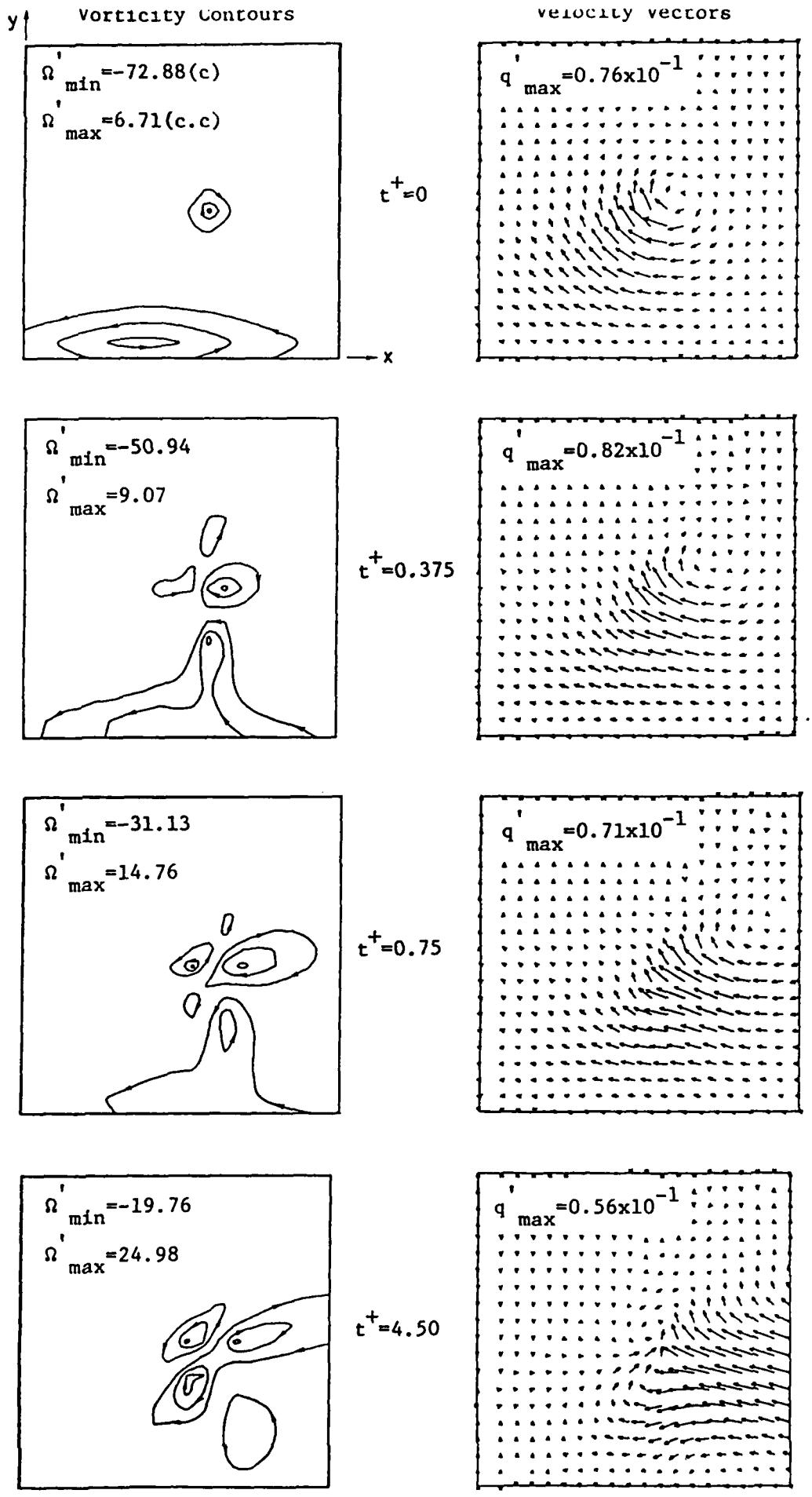

Fig.3 Variation of Flow Field (side view, $2z^+/\lambda_o^+ = 0$)

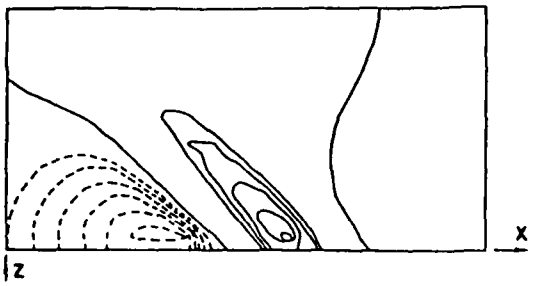

$t^+=0$, $y^+=0$

$C'_{p_{min}} = -868.51\times10^{-4}$ (<0, solid line)

$C'_{p_{max}} = 109.29\times10^{-4}$ (>0, dotted line)

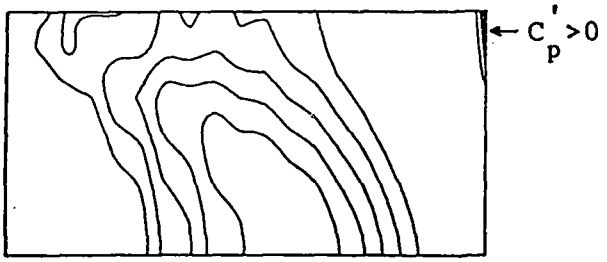

$t^+=0.375$, $y^+=0$

$C'_{p_{min}} = -53.95\times10^{-4}$

$C'_{p_{max}} = 1.72\times10^{-4}$

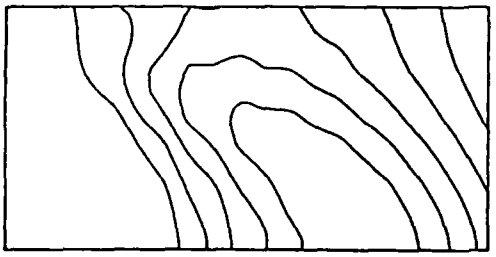

$t^+=0.75$, $y^+=0$

$C'_{p_{min}} = -49.48\times10^{-4}$

$C'_{p_{max}} = -2.87\times10^{-4}$

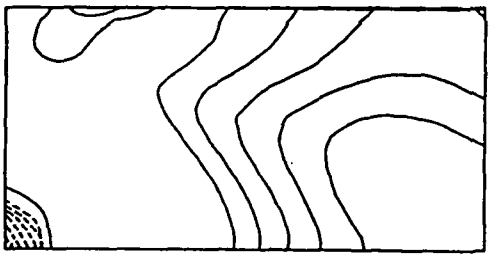

$t^+=2.625$, $y^+=0$

$C'_{p_{min}} = -35.46\times10^{-4}$

$C'_{p_{max}} = 0.73\times10^{-4}$

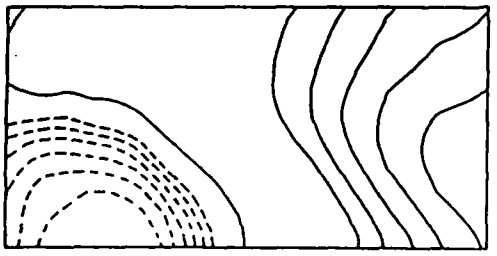

$t^+=4.50$, $y^+=0$

$C'_{p_{min}} = -26.20\times10^{-4}$

$C'_{p_{max}} = 9.61\times10^{-4}$

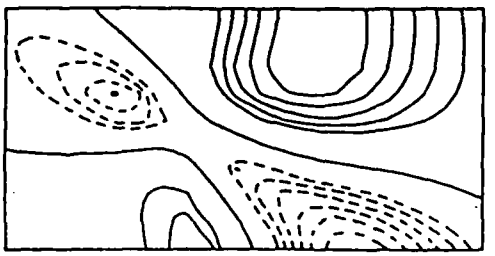

$t^+=4.50$, $y^+=6.25$

$C'_{p_{min}} = -68.35\times10^{-4}$

$C'_{p_{max}} = 65.33\times10^{-4}$

Fig.4 Contours of Fluctuating Pressure Coefficient ($C'_p = P' / \frac{1}{2}\rho U_\infty^2$)

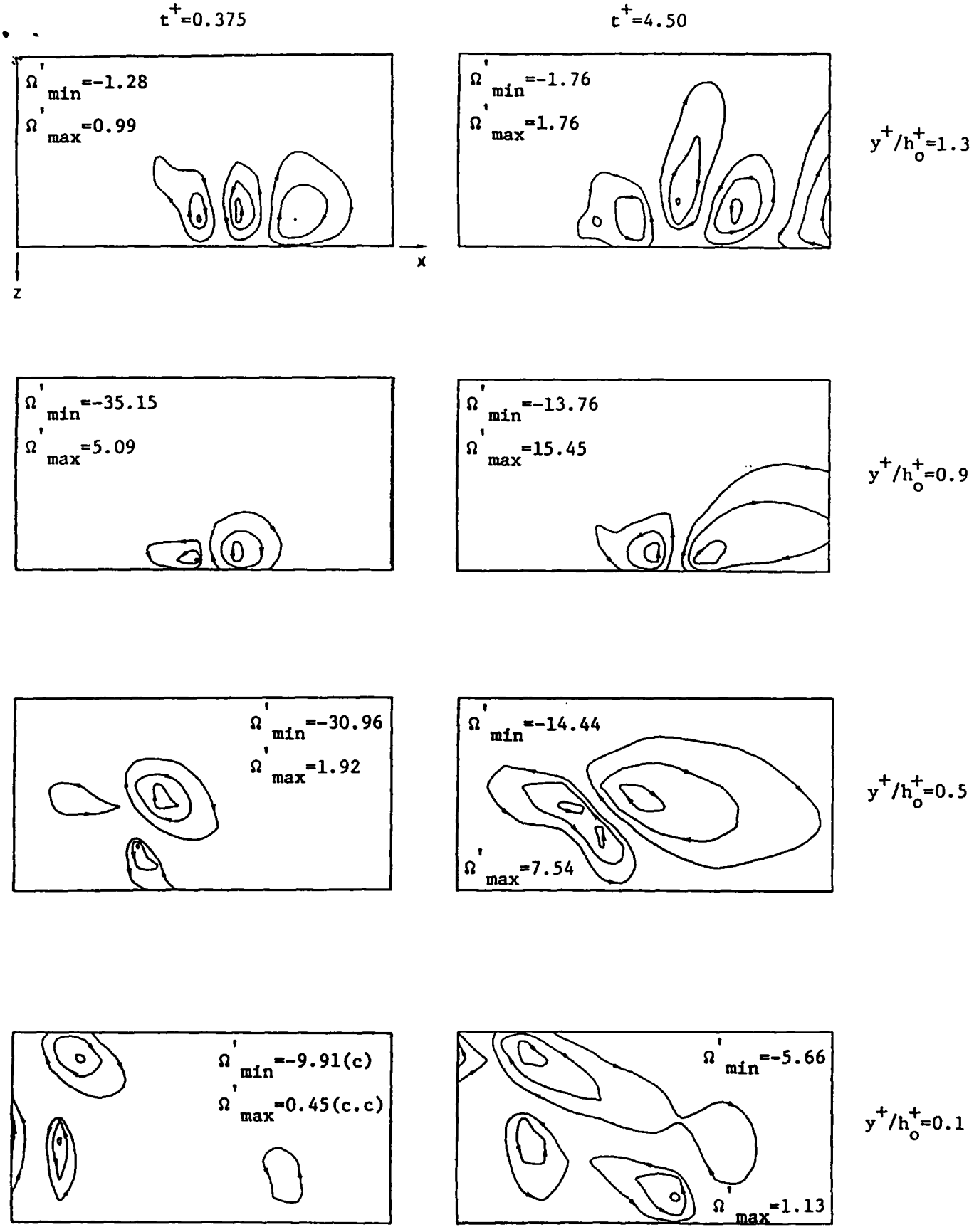

Fig.5 Contours of Vorticity Variation (top view)

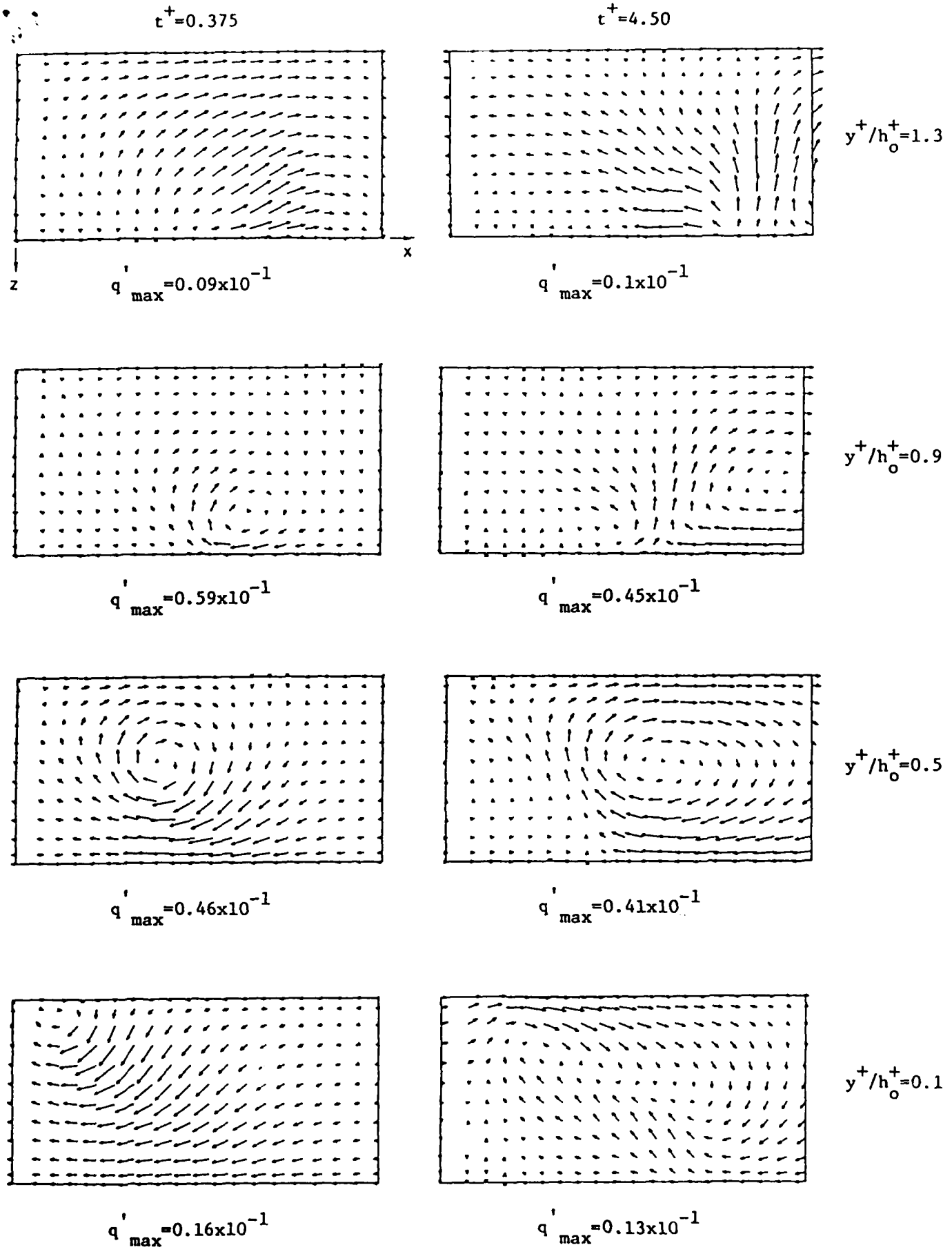

Fig.6 Vector Field of Velocity Variation (top view)

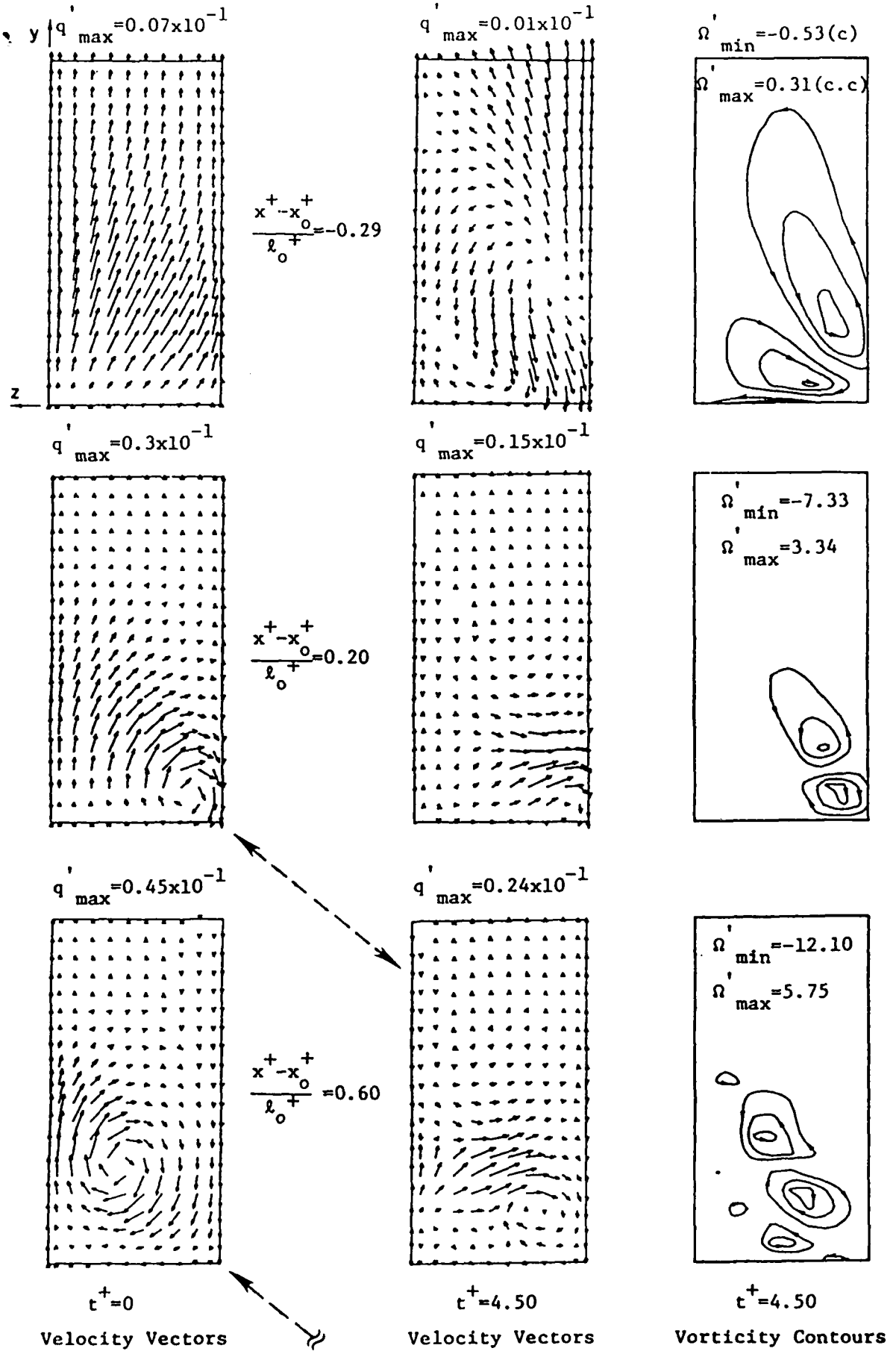

Fig.7a Variation of Flow Field (front view)

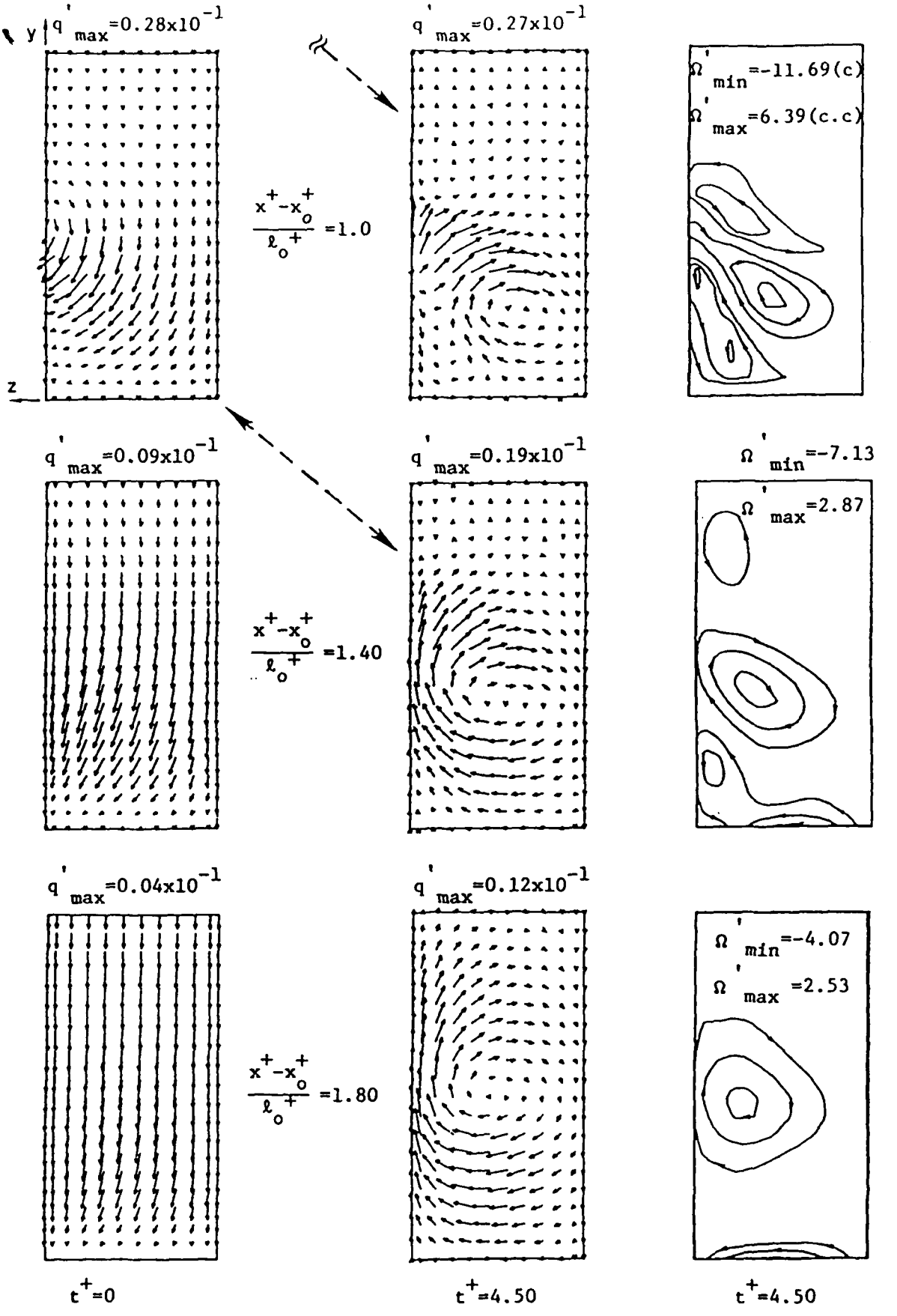

Fig.7b Variation of Flow Field (front view)

END

FILMED

1-86

DTIC